

# Speckle Imaging with the SOAR and the Very Large Telescopes

Sridharan Rengaswamy, Julien. H. Girard and Guillaume Montagnier

European Southern Observatory, Casilla 19001, Vitacura, Santiago, Chile

## ABSTRACT

Astronomical speckle imaging is a well established technique for obtaining diffraction limited images of binary and multiple stars, low contrast solar features and nearby extended objects such as comets and solar system planets, with large ground-based telescopes. We have developed a speckle masking code to reconstruct images of such objects from the corresponding specklegrams. This code uses speckle interferometry for estimating the Fourier amplitudes and bispectrum for estimating the Fourier phases. In this paper, we discuss a few technical issues such as: What is the photometric and astrometric accuracy that can be achieved with this code? What is the closest separation between the components of a binary star that can be clearly resolved with sufficient signal to noise ratio with this code? What is the maximum dynamic range? What kind of calibration schemes can be used in the absence of a bright calibrator close to the object of interest? We address these questions based on computer simulations. We present a few sample reconstructions from the real data obtained from the SOAR telescope. We also present the details of a technical feasibility study carried out with NACO-cube mode at the VLT.

**Keywords:** Speckle imaging, Triple correlation, High resolution imaging, speckle masking

## 1. INTRODUCTION

Achieving high angular resolution from ground based telescopes requires not only good sites with minimal image degradation, but also powerful image restoration techniques that are immune to the atmospheric turbulence. Speckle imaging<sup>1-3</sup> is one such technique, well suited for imaging with large telescopes at optical and near infrared wavelengths, with relatively less expensive hardware and software. In this paper, we explore the use of this technique with simulated and real data. In the next section, we provide the basic theory of speckle imaging. In section 3, we evaluate the performance of our speckle code through simulations. We used our code to reconstruct images of a few binary stars observed with the 4-m SOAR<sup>4,5</sup> telescope. These results are presented in section 4. In section 5, we present the results of the test observations performed to assess the feasibility of speckle imaging and data analysis with the NACO<sup>6,7</sup> cube mode data. In section 6, we briefly describe our speckle data simulation and analysis tools and, in section 7, we provide the summary of the results.

## 2. SPECKLE IMAGING: OBSERVATIONS AND ANALYSIS

### 2.1 Observations

A typical speckle imaging observation involves acquiring a series of images of object of interest (binary and multiple stars, extended objects like solar granulation, sunspots), each exposed for a duration shorter than the atmospheric coherence time, with a fast detector. A series of dark and flat frames are recorded, preferably, prior to, and/or after the target observation for calibrating the data. An spectral filter of suitable bandwidth (depending on the actual observing wavelength, typically 1 to 100 Å at optical wavelengths, a few thousand Å at near infrared wavelengths), is used depending upon the object under observation.

---

Further author information: (Send correspondence to R. Sridharan)

R. Sridharan: E-mail: srengasw@eso.org, Telephone: +56 (0)2 463 3084

## 2.2 Analysis

All the images of a burst are processed together to reconstruct an image that would be a ‘close’ representation of the object during the time interval over which the burst was recorded. An intrinsic assumption here is that the object does not evolve during this time interval (nearly extended objects like the solar granulation, sunspots, small scale solar photospheric structures may require several quick bursts to study their time evolution.). The basic processing required for reconstructing an image (of size of the order of an isoplanatic patch) is described below.

The instantaneous image  $i(\mathbf{x})$  formed by a telescope is the convolution ( $\odot$ ) of the object  $o(\mathbf{x})$  and the point spread function  $p(\mathbf{x})$  of the system.<sup>8</sup>

$$i(\mathbf{x}) = o(\mathbf{x}) \odot p(\mathbf{x}) + n(\mathbf{x}), \quad (1)$$

where  $\mathbf{x}$  is two dimensional position at the detector plane and  $n(\mathbf{x})$  is the noise in the measurement. The Fourier amplitudes  $|O(\mathbf{f})|$  and phases  $\phi_O(\mathbf{f})$  of the object are obtained by separate processing techniques and the object is restored by performing a simple Fourier inversion.

### 2.2.1 Recovery of Fourier Amplitudes

First, the modulus squared Fourier transform of the images  $|I(\mathbf{f})|^2$  are averaged<sup>1</sup> over several realizations of the atmosphere (ensemble average)\*.

$$\langle |I(\mathbf{f})|^2 \rangle = |O(\mathbf{f})|^2 \langle |P(\mathbf{f})|^2 \rangle + \langle |N(\mathbf{f})|^2 \rangle. \quad (2)$$

The noise power spectrum  $\langle |N(\mathbf{f})|^2 \rangle$  is estimated separately and subtracted from the ensemble average to obtain a noise corrected power spectrum  $\langle |I'(\mathbf{f})|^2 \rangle$ . The function  $\langle |P(\mathbf{f})|^2 \rangle$  is the modulus squared frequency response of the system (telescope and the atmosphere) at the time of observation. The Fourier amplitudes of the object are recovered using the relation

$$|O(\mathbf{f})| = \sqrt{\frac{\langle |I'(\mathbf{f})|^2 \rangle}{\langle |P(\mathbf{f})|^2 \rangle}} \cdot F, \quad (3)$$

where  $F$  is a filter used to weight the Fourier amplitudes

### 2.2.2 Recovery of Fourier Phases

The Fourier phases of the complex signal  $O(\mathbf{f})$  representing the Fourier transform of the object are recovered from the ensemble averaged bispectrum of the recorded images<sup>2</sup> defined as

$$\begin{aligned} \langle b(\mathbf{f}_1, \mathbf{f}_2) \rangle &= \langle I(\mathbf{f}_1) \cdot I(\mathbf{f}_2) \cdot I^*(\mathbf{f}_1 + \mathbf{f}_2) \rangle \\ &= O(\mathbf{f}_1) \cdot O(\mathbf{f}_2) \cdot O^*(\mathbf{f}_1 + \mathbf{f}_2) \langle P(\mathbf{f}_1) \cdot P(\mathbf{f}_2) \cdot P^*(\mathbf{f}_1 + \mathbf{f}_2) \rangle + N_b, \end{aligned} \quad (4)$$

where  $N_b$  is the noise term. The quantity within the angular brackets on the right is observed to be a real quantity,<sup>3</sup> making the ensemble averaged bispectrum a real quantity, in the absence of noise. The phase of the ensemble averaged bispectrum  $\phi_b(\mathbf{f}_1, \mathbf{f}_2)$  is, then<sup>†</sup>,

$$\phi_b(\mathbf{f}_1, \mathbf{f}_2) = \phi_O(\mathbf{f}_1) + \phi_O(\mathbf{f}_2) - \phi_O(\mathbf{f}_1 + \mathbf{f}_2). \quad (5)$$

The Fourier phases of the object at frequency  $\mathbf{f} = \mathbf{f}_1 + \mathbf{f}_2$  can now be estimated as

$$\phi_O(\mathbf{f}) = \phi_O(\mathbf{f}_1) + \phi_O(\mathbf{f}_2) - \phi_b(\mathbf{f}_1, \mathbf{f}_2). \quad (6)$$

---

\*the cross terms vanish, as the noise is uncorrelated with the signal

†We use the notation  $\phi_b(\mathbf{f}_1, \mathbf{f}_2)$  to denote  $\phi_{\langle b(\mathbf{f}_1, \mathbf{f}_2) \rangle}$  throughout this paper.

### 3. SIMULATIONS

We performed computer simulations to evaluate the performance of our code in observing binary stars. What follows is the description of the procedure used in our simulations. In short, the simulation includes a model of the source (object), a model of the atmospheric turbulence, and a model of the instrument/detector system.

#### 3.1 Source model

The source model is essentially simulation of a model binary star. The astrometric (separation between the stars, and the position angle) and the photometric (spectral type and the magnitude) parameters were defined as free or user defined parameters of the model. The spectral energy distributions (SEDs) of the stars were adopted from Pickles<sup>9</sup> model spectra and were scaled according to the brightness of the stars. The zero points were adopted from Bessel and Brett.<sup>10</sup>

#### 3.2 The atmospheric turbulence model

The atmospheric turbulence was assumed to be of von-Korman<sup>8,11</sup> type with a finite outer scale length of turbulence. The strength of the turbulence was defined in terms of the seeing (or the Fried's parameter( $r_0$ ) at zenith, at 550 nm) parameter. The wind speed (thus, the coherence time) and the telescope airmass were the also used as input parameters. As the current simulations were mostly aimed at the use of NACO for speckle imaging, we adopted the median value (22 m) of the outer scale length of turbulence obtained at Paranal.<sup>12</sup> The effect of turbulence was simulated in terms of a "phase-screen" that represents the perturbed wavefront at the pupil. A single large phase screen was generated and was "blown" past the telescope aperture to obtain a time sequence of perturbed wavefronts.

#### 3.3 Instrument model

The simulations were performed for a telescope diameter of 8 m. The instrument, filter and the detector parameters were adopted from the NACO/CONICA<sup>‡</sup> instrument/camera with the detector gain of 11 e/ADU and a rms readout noise of 4.2 ADU. Simulations were performed at J, H and Ks bands.

#### 3.4 Simulation of specklegrams

The specklegrams were obtained as the modulus squared Fourier transform of the perturbed wavefront at the pupil. The normalized specklegram was convolved with the binary model source to obtain the specklegram corresponding to the binary. Poisson noise was simulated by adding the square root of a Poisson distributed random variate with mean value of the signal at each pixel. The readout noise was simulated by adding a normally distributed random variate with standard deviation of 4.2 (ADU).

#### 3.5 Results

In principle, there exist a wide range of parameters (in terms of photometry and astrometry of the targets, atmospheric conditions such as the seeing and the coherence time (or the wind speed)) for the simulations. Here we present the results corresponding to mediocre observing conditions which will help us to understand, by extrapolation, what can be expected under better or worse conditions. These results were obtained with the following parameters: (a) simulations in the J band, (b) seeing (at 500nm) of 1.5", airmass of 1.2, and wind speed of 10m/s, (c) exposure time of 80 ms, telescope diameter of 8m and (d) M dwarf binaries as source models. Figures 1 to 4 indicate speckle reconstructions obtained with our code under these conditions. These results can easily be extended to what can be expected under better seeing conditions and in the Ks band, where the performance is expected to be better.

---

<sup>‡</sup><http://www.eso.org/sci/facilities/paranal/instruments/naco/inst/conica.html>

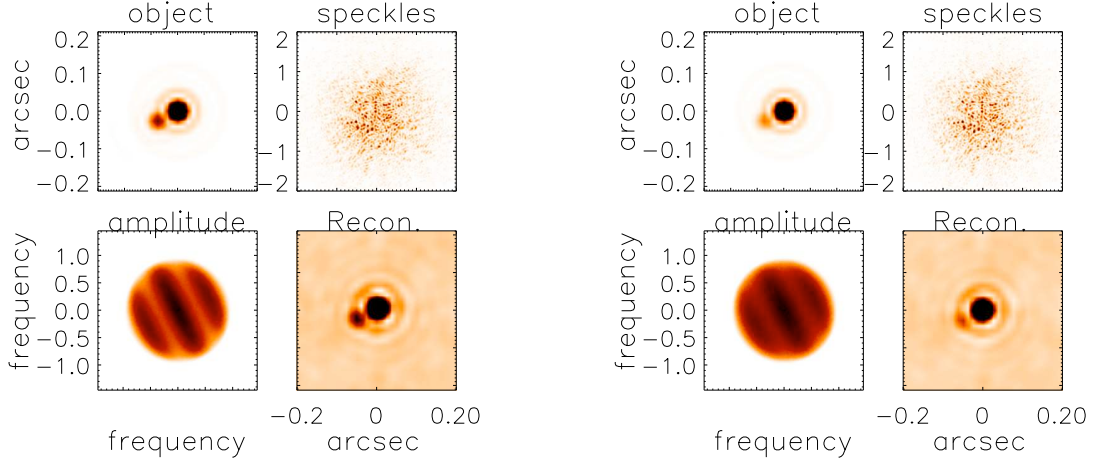


Figure 1. **Left:** The top left panel indicates a simulated binary with 60 mas separation, 110 degrees position angle and  $\Delta m=2$ . The top right panel indicates one of the simulated specklegrams. The bottom left panel indicates the Fourier amplitude spectrum of the reconstruction. The bottom right panel indicates the speckle reconstruction. **Right:** Similar panels, but for  $\Delta m=3$ . The secondary (component of the binary) is clearly visible in both the cases.

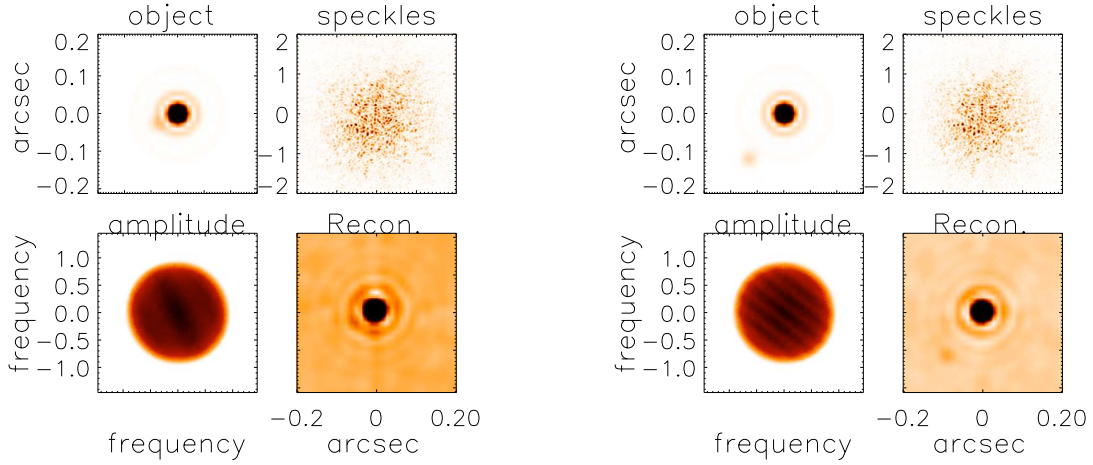


Figure 2. **Left:** The top left panel indicates a simulated binary with 60 mas separation, 110 degrees position angle and  $\Delta m=4$ . The top right panel indicates one of the simulated specklegrams. The bottom left panel indicates the Fourier amplitude spectrum of the reconstruction. The bottom right panel indicates the speckle reconstruction. The secondary is not clearly visible in the reconstruction. **Right:** Similar panels, but for a binary with 150 mas separation, 140 degrees position angle and  $\Delta m=4$ . The secondary is clearly visible in this case.

### 3.5.1 Astrometric and Photometric accuracy & the dynamic range

In all our simulations, we could obtain the relative separation of the binaries with an accuracy of much less than a pixel and hence a very good accuracy on the position angle.. The photometric accuracy of individual stars

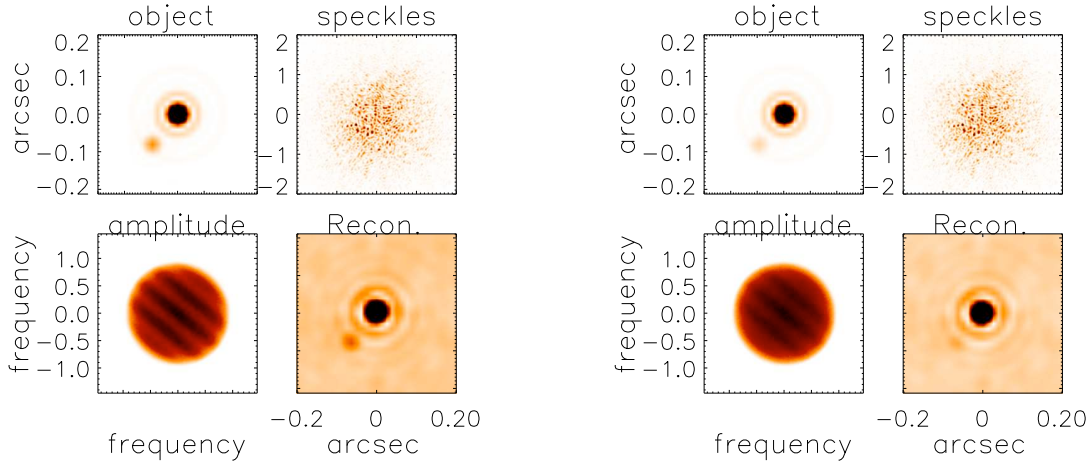


Figure 3. **Left:** The top left panel indicates a simulated binary with 100 mas separation, 140 degrees position angle and  $\Delta m=3$ . The top right panel indicates one of the simulated specklegrams. The bottom left panel indicates the Fourier amplitude spectrum of the reconstruction. The bottom right panel indicates the speckle reconstruction. **Right:** Similar panels, but for  $\Delta m=4$ . The secondary is clearly visible in both the cases.

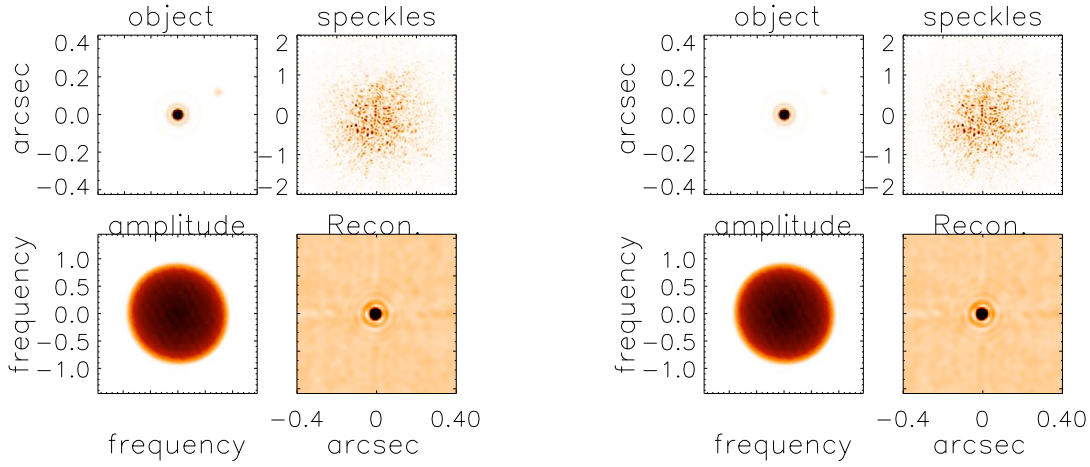


Figure 4. **Left:** The top left panel indicates a simulated binary with 250 mas separation, 300 degrees position angle and  $\Delta m=4$ . The top right panel indicates one of the simulated specklegrams. The bottom left panel indicates the Fourier amplitude spectrum of the reconstruction. The bottom right panel indicates the speckle reconstruction. **Right:** Similar panels, but for  $\Delta m=5$ . The secondary is not clearly visible in both the cases.

were widely different. However, a slightly better accuracy could be obtained in the relative photometry (ratio of brightness). Table 1 indicates the astrometric and photometric accuracies. The maximum dynamic range is at least 3 magnitudes between the primary and the secondary under  $1.5''$  seeing. Also, the relative photometry decreases as the component becomes fainter.

Table 1. This table indicates the typical astrometric and photometric accuracies obtained with our speckle reconstruction code.  $\Delta r$  is the binary separation,  $\Delta m$  is the magnitude difference,  $d(\Delta m)$  is the error in the magnitude difference. Only when the secondary is clearly visible in the reconstruction, it was declared as ‘detected’.

$\Delta r$ (mas)	$\Delta m$	$d(\Delta m)$	Detection
60	2	0.25	Yes
	3	0.665	Yes
	4	1.368	No
100	3	0.07	Yes
	4	1.07	Yes
150	4	0.04	Yes
250	4	0.889	No
	4	0.1	No

### 3.5.2 Calibrations

Our simulation tool allows us to generate a synthetic speckle transfer function corresponding to the observing conditions (seeing, wind speed, wavelength) and use it for the deconvolution when there are no bright nearby calibrators near the target of interest. We estimate the transfer function through numerical simulation of the sequence of specklegrams. In practice, it will be necessary to observe a few bright calibrators in different directions (zenith distances) on the sky to account for the effects of static aberrations/pointing errors on the speckle transfer function and hence obtain a better relative photometry.

## 4. SPECKLE RECONSTRUCTIONS FROM THE SOAR DATA

We also tested our code by reconstructing the speckle data obtained with the 4-m SOAR telescope in Chile.<sup>5</sup> The data were obtained with ‘y’(550 nm) and  $H_\alpha$  (656 nm) filter with an integration time of 20 ms. Figures 5 and 6 show some of the reconstructions obtained with our code.

## 5. SPECKLE IMAGING WITH THE NACO AT THE VLT

We performed speckle observations with the NACO at the VLT on January 28, 2010, to evaluate the feasibility of speckle imaging with the cube mode of NACO.

### 5.1 Observations & Analysis

We observed binary stars HIP24800, HIP35415, and WT460, with the seeing varying between 0.42'' and 1.25''. For the first two binaries, we also observed nearby calibrators HD34738 and HD57757 respectively. As we could not observe a calibrator for WT460, we used a synthetic speckle transfer function generated with our simulating tool for deconvolution. Figures 7 to 9 show the reconstructed images.

### 5.2 Results

#### 5.2.1 SCI\_HIP 24800 and CAL\_HD 34738:

HIP 24800 is a binary with J magnitude of about 7. We selected this SCI-CAL pair, purely as a ‘simple test’ for the observations and the software and this has served the purpose. We could obtain good reconstructions and hence test both the observing procedure and the software, including their repeatability. The mean separation between the stars in this binary is  $161.7 \pm 6.5$  mas in the J band and 161.5 mas in the Ks band. The mean position angle is  $19.2^\circ \pm 0.8^\circ$ ,  $18.43^\circ$  respectively. The ratio of peak brightness of the primary and the secondary is  $2.27 \pm 0.11$ .

The bottom left images in each panel of Figures 7 to 9 show the speckle reconstructed images. The top panel shows the “worst” and the “best” images of the burst. The best images was identified as the one having highest fourth moment. The bottom right panel shows the average long exposure image obtained from the burst.

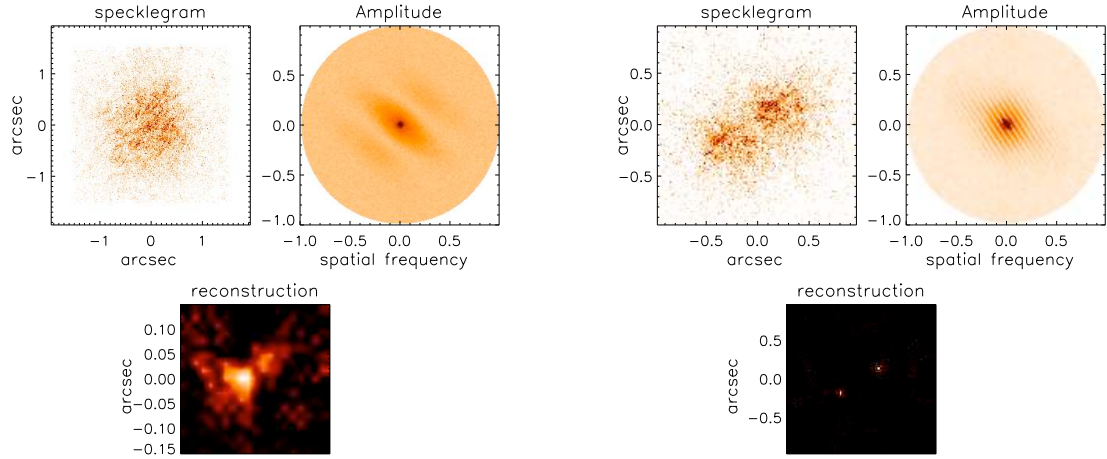


Figure 5. **Left:** The top left panel indicates one of the specklegrams (at 550 nm) of the burst. The top right panel indicates the Fourier amplitude spectrum. The bottom panel indicates speckle reconstruction (SN.006). The binary separation is about 50 mas. It is the ‘close’ binary we could resolve. **Right:** The top left panel indicates one of the specklegrams (at 550 nm) of the burst. The top right panel indicates the Fourier amplitude spectrum. The bottom panel indicates speckle reconstruction (SN.087). The binary separation is  $0.6''$  and the magnitude difference is about 0.48.

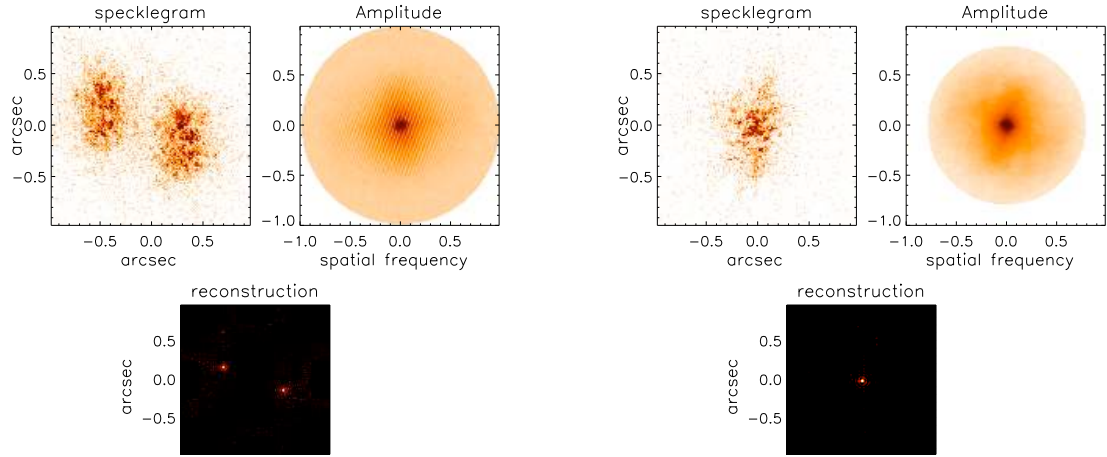


Figure 6. **Left:** The top left panel indicates one of the specklegrams (at 550 nm) of the burst. The top right panel indicates the Fourier amplitude spectrum. The bottom panel indicates speckle reconstruction (SN.177). The binary separation  $0.82''$  and the magnitude difference is about 0.8. **Right:** The top left panel indicates one of the specklegrams (at 656 nm) of the burst. The top right panel indicates the Fourier amplitude spectrum. The bottom panel indicates speckle reconstruction (SN.210). We do not clearly see any component star other than the primary.

### 5.2.2 SCI.HIP 35415 and CAL.HD 57757:

We selected this SCI-CAL pair to test the dynamic range, which was expected to be  $\delta m=4$  between primary and the secondary. The separation between the stars in this binary is 125 mas in the J band and 114 mas in the K

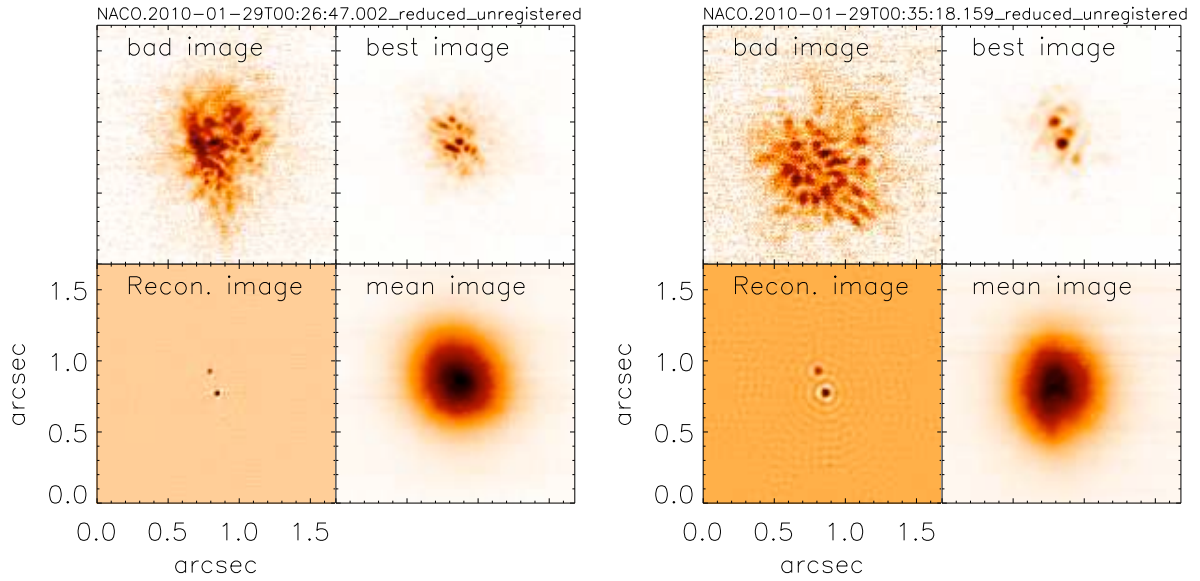


Figure 7. **Left:** Images of HIP24800 in J band. Top Left: Worst image of the data cube. Top Right: Best image of the data cube. Bottom Left: speckle reconstruction Bottom Right: Average image of the data cube. The images have been scaled to 0-255, and reversed in contrast (0=brightest, 255=faintest) and displayed with pseudo-color. **Right:** Similar images, in the Ks band.

band; The position angle is  $-58^\circ$  and  $-54^\circ$  respectively. The left panel in Figure 8 shows images of HIP 35415 in J band, and the right panel shows images in Ks band. The peak brightness ratio between the primary and the secondary is 2.14.

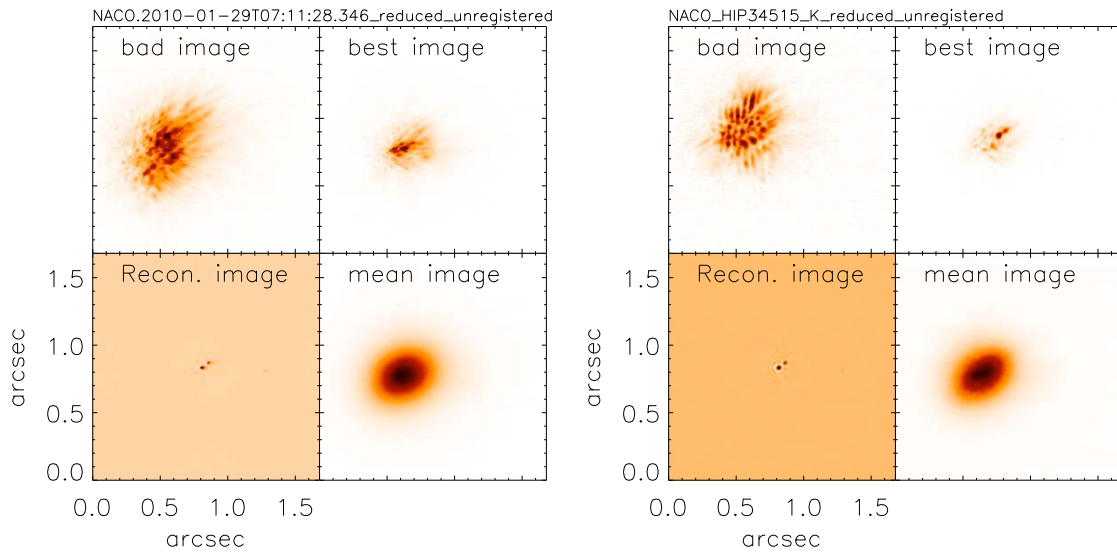


Figure 8. **Left:** Images of HIP35415 in J band. Top Left: Worst image of the data cube. Top Right: Best image of the data cube. Bottom Left: speckle reconstruction Bottom Right: Average image of the data cube. The images have been scaled to 0-255, and reversed in contrast (0=brightest, 255=faintest) and displayed with pseudo-color. **Right:** Similar images, in the Ks band.

### 5.2.3 SCI\_WT460:

Figure 9 shows the speckle reconstructions in J and Ks band respectively, along with the best, bad, long exposure images. Again, the images have been re-scaled and reverse contrasted. As mentioned earlier, we did not observe a calibrator close to this binary. Therefore, we used a synthetic speckle transfer function for deconvolution. The secondary is clearly visible in the reconstruction. The average separation between the stars of this binary is 310 mas, the position angle is  $-50^\circ$  and the brightness ratio is 14.9 in the J band. This corresponds to a magnitude difference of 2.9. The brightness ratio is 9.05 in the Ks band corresponding to the magnitude difference of 2.3.

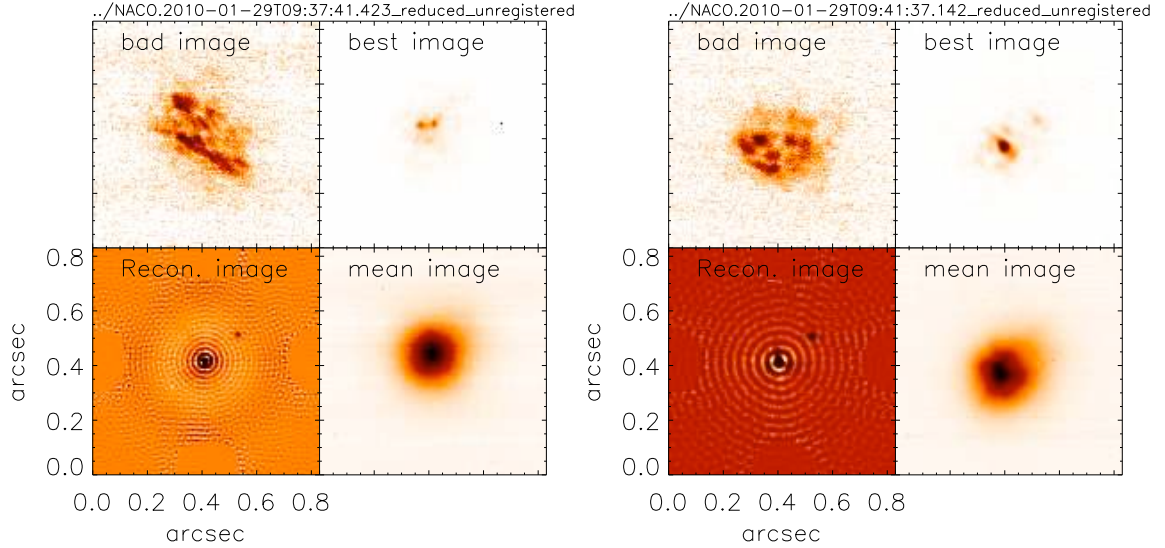


Figure 9. **Left:** Images of WT460 in J band. Top Left: Worst image of the data cube. Top Right: Best image of the data cube. Bottom Left: speckle reconstruction Bottom Right: Average image of the data cube. The images have been scaled to 0-255, and reversed in contrast (0=brightest, 255=faintest) and displayed with pseudo-color. **Right:** Similar images in Ks band

### 5.2.4 Strehl Ratios

As described earlier, the speckle reconstruction yields the “object” intensity distribution on the sky (of course sampled at the spatial sampling of the detector). This is quantitatively different from the “image” intensity distribution (which is object convolved with the response of the telescope under ideal seeing conditions) or the point spread function obtained in normal or adaptive optics imaging. Thus, prior to obtaining the Strehl ratios, we convolved the speckle reconstructions with an ideal synthesized PSF of the telescope. We estimated Strehl ratio as the ratio of volume under transfer function to the volume under the transfer function of an ideal (synthesized) PSF. The Strehl ratios were in the range of 0.6 to 0.8 for bright targets in the J band and slightly higher in the Ks band. As speckle image reconstruction “corrects” for the phase aberrations up to infinite order (unlike the adaptive optics imaging, which corrects the phase aberrations up to a finite order of equivalent Zernike modes), we obtain higher Strehl ratios than the adaptive optics imaging or normal imaging, particularly in the J band.

### 5.2.5 Comparison with AO corrected images

Since we recorded AO corrected images (near simultaneously), analyzed the AO corrected data cube and obtained an image. Figure 12 shows a comparison between the AO corrected image and the speckle reconstruction. The images have been re-scaled (between 0 and 255) and their contrast has been reversed for the sake of display. Again, we should be careful in interpreting the results, as the AO corrected image is in the image plane and the speckle reconstruction is on the sky plane. After accounting for this difference, we find that speckle imaging gives a Strehl of 0.7 and 0.9 in J and Ks bands whereas AO gives a Strehl of 0.3 and 0.5 in J and Ks bands respectively. Also, it should be noted that for the object observed with at high airmass, and with a median seeing speckle imaging gives a Strehl of 0.4 in J band and 0.65 in K band.

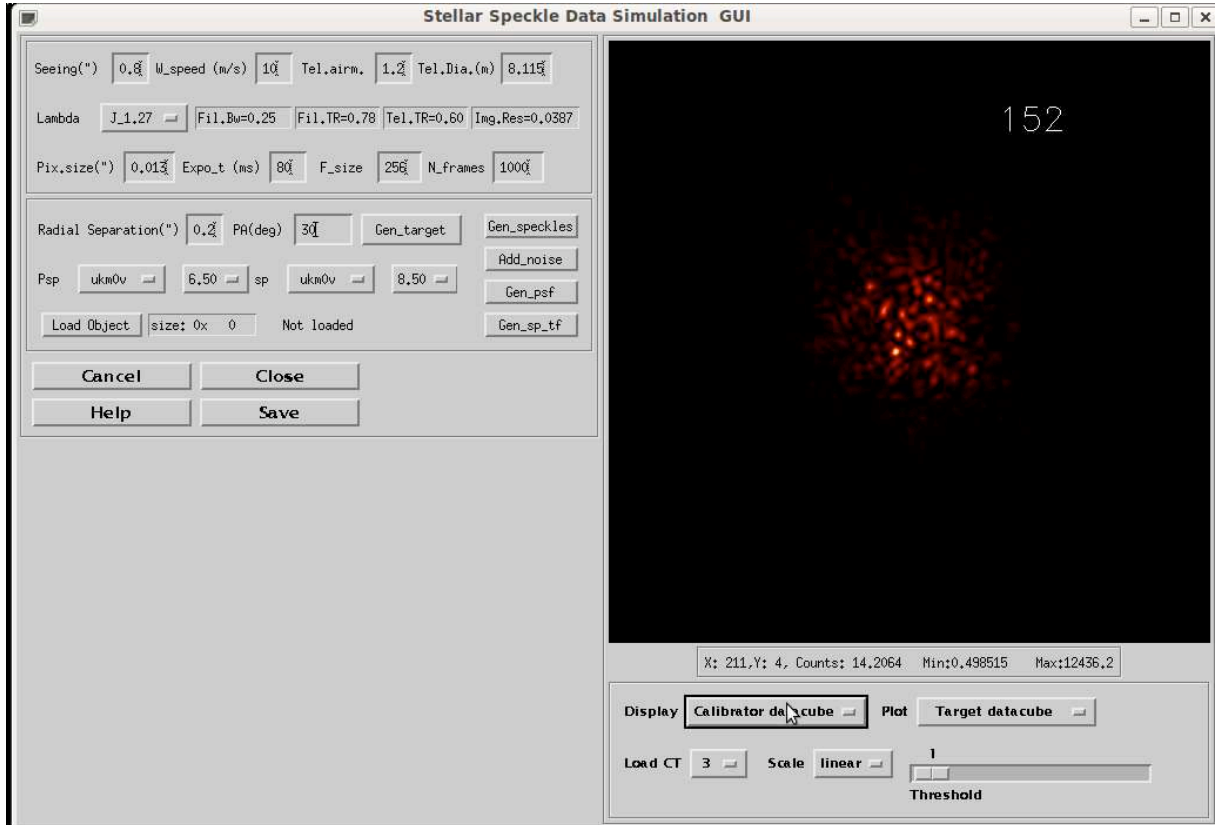


Figure 10. Screen-shot of the Speckle simulator developed to simulate speckle imaging observations with the NACO.

## 6. SIMULATION AND ANALYSIS TOOLS

We have developed a simulation tool which can be used to simulate speckle imaging data, particularly, the data that can be expected from the NACO at the VLT. Currently most of the parameters of the simulations are adopted from the NACO at the VLT. Figure 10 shows the screen-shot of the simulation tool. The seeing, wind speed, telescope airmass, telescope diameter, wavelength and filter characteristics, detector characteristics, exposure time, number of frames, size (field-of-view) in pixel units are the user defined parameters. For simulating a binary star, the user has to define the parameters of the binary such as separation, position angle and the spectral types of the stars. For simulating a complicated object (triple star or extended objects), the input data can be exported in FITS format. A series of specklegrams, the point spread function of the resulting long exposure image and the speckle transfer functions are the output parameters available for the users. Any of the input or output parameters can be displayed on the screen for visual inspection. Figure 11 shows the screen-shot of the speckle data analysis tool. The user has to load the target and calibrator data cubes (or calibrator amplitude spectrum, if available), and enter the pixel size, resolution, wavelength of observation and the telescope diameter. In principle, the users can obtain any or all of the following: (a) Ensemble averaged Fourier transform, (b) Autocorrelation of the object (c) A phase only reconstruction and (d) A full image reconstruction. There are several parameters which can be selected with a little experience. They are: (a) correction for photon noise- this is useful when the data is photon noise limited, (b) phase consistency filter for weighting the bispectrum, (c) use of Fourier phases of the average image as a boundary condition to start the recursive phase reconstruction, (d) ability to or not to calibrate the data, (f) apodizing the individual frames with either a 20% or 100% modified hanning function, (g) truncating the bispectrum at the desired number (to be selected among the options available) and (h) eliminating the Fourier phases that differ from the mean by 1,2 or 3 sigma level at each spatial frequency. A wide range of parameters of the input images and the reconstructed image can be displayed and visually inspected. This tool (a FORTRAN code and IDL widget wrapper) is easy

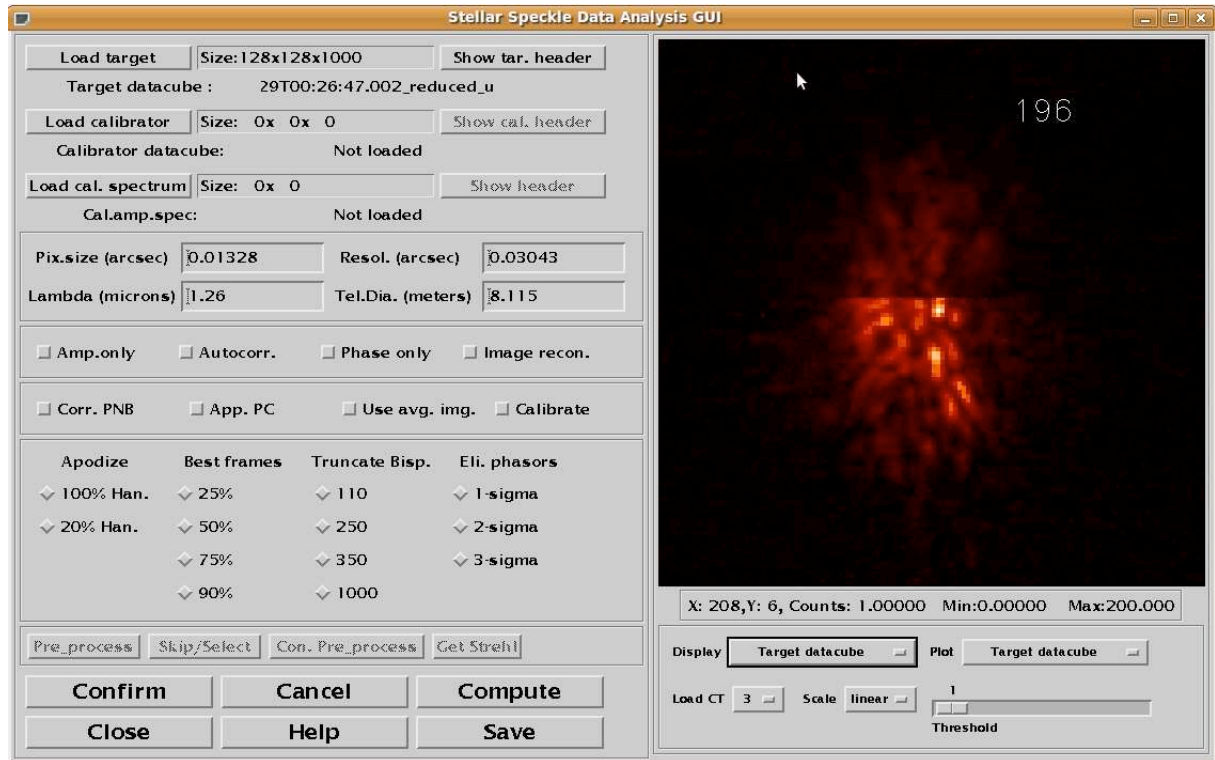


Figure 11. Screen-shot of the Speckle analyzing software tool.

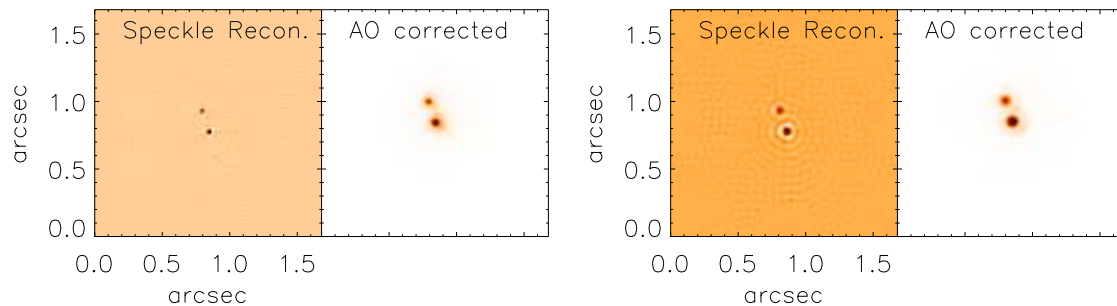


Figure 12. Comparison of Speckle reconstruction with AO corrected images. The images have been re-scaled between 0 and 255 and their contrast have been reversed. The AO corrected image was obtained from 5 different data cubes each with a different offset. Thus the background is averaged out and is smooth; so it appears almost white. The speckle reconstruction, on the other hand contains small non-zero fluctuations and hence it shows background variations.

to use, with a little experience<sup>§</sup>.

<sup>§</sup>Contact the author for using the code and/or for further details.

## 7. SUMMARY

Our speckle analysis software is capable of obtaining diffraction limited images of binary stars. We obtain the relative separation of the binary stars with a very good accuracy (less than a pixel). A dynamic range of  $\Delta m=3$  can be achieved at 60 mas separation, in the J band, under 1.5" seeing. The maximum dynamic range is of the order of 3 to 4 magnitudes under the same conditions. We do not have reliable estimate of the absolute photometry, but the relative photometry is accurate, at least when the components differ by less than two magnitudes. We have been able to achieve up to 50 mas resolution at 550 nm with the SOAR telescope data. We have established that speckle imaging can be performed with the cube mode of the NACO at the VLT. The software has been tested extensively. We have also developed a simulator to estimate the expected performance of speckle imaging under a wide range of conditions, at different wavelengths.

## ACKNOWLEDGMENTS

We thank A. Tokovinin, for kindly providing us the SOAR speckle data presented in this paper. We thank A. Kaufer, the director of LPO for granting us time to perform tests to assess the feasibility of speckle imaging with the NaCo Cube mode at the VLT.

## REFERENCES

- [1] Labeyrie, A., "Attainment of Diffraction Limited Resolution in Large Telescopes by Fourier Analysing Speckle Patterns in Star Images," *Astron. and Astrophysics* **6**, 85–87 (May 1970).
- [2] Weigelt, G. P., "Modified astronomical speckle interferometry 'speckle masking'," *Optics Communications* **21**, 55–59 (Apr. 1977).
- [3] Lohmann, A. W., Weigelt, G., and Wirtzner, B., "Speckle masking in astronomy - Triple correlation theory and applications," *Appl. Optics* **22**, 4028–4037 (Dec. 1983).
- [4] Tokovinin, A. and Cantarutti, R., "First speckle interferometry at soar telescope with electron-multiplication ccd," *Pub. Astron. Soc. Pacific* **120**, 170–177 (Feb. 2008).
- [5] Tokovinin, A., Mason, B. D., and Hartkopf, W. I., "Speckle interferometry at the blanco and soar telescopes in 2008 and 2009," *Astron. Journal* **139**, 743–756 (Feb. 2010).
- [6] Lenzen, R., Hartung, M., Brandner, W., Finger, G., Hubin, N. N., Lacombe, F., Lagrange, A., Lehnert, M. D., Moorwood, A. F. M., and Mouillet, D., "NAOS-CONICA first on sky results in a variety of observing modes," in [*Society of Photo-Optical Instrumentation Engineers (SPIE) Conference Series*], M. Iye & A. F. M. Moorwood, ed., *Presented at the Society of Photo-Optical Instrumentation Engineers (SPIE) Conference* **4841**, 944–952 (Mar. 2003).
- [7] Rousset, G., Lacombe, F., Puget, P., Hubin, N. N., Gendron, E., Fusco, T., Arsenault, R., Charton, J., Feautrier, P., Gigan, P., Kern, P. Y., Lagrange, A., Madec, P., Mouillet, D., Rabaud, D., Rabou, P., Stadler, E., and Zins, G., "NAOS, the first AO system of the VLT: on-sky performance," in [*Society of Photo-Optical Instrumentation Engineers (SPIE) Conference Series*], P. L. Wizinowich & D. Bonaccini, ed., *Presented at the Society of Photo-Optical Instrumentation Engineers (SPIE) Conference* **4839**, 140–149 (Feb. 2003).
- [8] Roddier, F., "The effect of atmospheric turbulence in optical astronomy," *Progress in Optics* **XIX**, 281–376 (1981).
- [9] Pickles, A. J., "A Stellar Spectral Flux Library: 1150-25000 Å," *Pub. Astron. Soc. Pacific* **110**, 863–878 (July 1998).
- [10] Bessell, M. S. and Brett, J. M., "JHKLM photometry - Standard systems, passbands, and intrinsic colors," *Pub. Astron. Soc. Pacific* **100**, 1134–1151 (Sept. 1988).
- [11] Goodman, J. W., [*Statistical Optics*], John Wiley & Sons (1985).
- [12] Martin, F., Conan, R., Tokovinin, A., Ziad, A., Trinquet, H., Borgnino, J., Agabi, A., and Sarazin, M., "Optical parameters relevant for High Angular Resolution at Paranal from GSM instrument and surface layer contribution," *Astron. and Astroph. Suppl. Series* **144**, 39–44 (May 2000).